https://dx.doi.org/10.4314/ijs.v25i2.9
Ife Journal of Science vol. 25, no. 2 (2023)

HYDROCARBON DETECTION AND DEPOSITIONAL ENVIRONMENT PROGNOSIS IN THE NIGER DELTA - INTEGRATED INSIGHTS FROM LOG AND SEISMIC AVO-INVERSION ATTRIBUTES

Falebita, D.*, Ojo, A. and Akintokewa, O.
Department of Geology, Obafemi Awolowo University, Ile-Ife, Nigeria.
*Corresponding Author's Email: delefale@oauife.edu.ng
(Received: 30th June, 2023; Accepted: 12th August, 2023)

ABSTRACT

This study demonstrates the effectiveness of integrated seismic analysis and petrophysically constrained AVO-inversion for reservoir evaluation and assessment of hydrocarbon potential and depositional environment in the Niger Delta. It is aimed at improved prediction of reservoir fluid, lithology, and ultimately the hydrocarbon prospects, with reduced uncertainties. The results delineate the characteristics of the reservoir sands, highlight major facies heterogeneities, unravel prolific stratigraphic features (such as channels, fan lobes), depositional fairways and provide insight into the mapped geology. These are expected to consequently reduce the uncertainties associated with the prospects for economic decision making.

Keywords: Petrophysics, Hydrocarbon detection, Niger delta, AVO-Elastic inversion attributes, Depositional environment prognosis.

INTRODUCTION

Delineation of subsurface heterogeneity in reliable reservoir description for the appraisal of hydrocarbon potential is becoming increasingly complex and requiring multi-level approach. Inadequate understanding of the fundamental characteristics of these spatially-varying heterogeneous reservoir properties such as lithology, pore fluids and saturation among others (Mukerji et al., 2001) results in poor appraisal of prospects and low production performance. So, an enhanced integration of datasets from seismic and well logs for reservoir properties mapping is a requisite for optimal economic returns in diverse petroleum reservoirs and depositional environments (Russell *et al*., 1997; Schuelke *et al*., 1998, Brown *et al*., 2004; Bose *et al*., 2004). Reservoir characterization has been demonstrated to enhance the lateral prediction of lithology and modelling of the internal reservoir architecture while seismic, sedimentological, petrophysical and reservoir engineering information have been methodically combined to give a very detailed reservoir evaluation (Soldo *et al*., 2001, Huang, 2001). Also, seismic inversion techniques have been proven to be very effective tools for facilitating integration of datasets and production of reservoir characterization (Bahorich and Farmer, 1995; Connolly, 1999; El-Mowafy and Marfurt, 2008). In addition, seismic attributes and amplitude variation with offset (AVO) have been used in lithological and fluid discrimination (Hilterman, 1990; Chopra and Pruden, 2003; Rauch-Davies *et al*., 2003; Eissa and Castagna, 2003; Aikulola *et al*., 2004). Moreover, spectral decomposition, coherence and other edge-detection attributes integrated together have been helpful in highlighting important channels (Partyka *et al*., 1999; Michael *et al*., 2003, Paulo *et al*., 2003; Chopra and Marfurt, 2005).

This study, therefore, appraises the hydrocarbon sands in the study location using a detailed integration of datasets from logs, geologic model, seismic AVO attributes and inversion. This is with a view to providing a robust prediction of reservoir fluid, lithology, and ultimately the hydrocarbon potential, with reduced uncertainties. The main petroleum interval in the study location is the Agbada Formation of the Tertiary system (Figure 1a) within the Niger Delta petroleum province (Figure 1b *inset*). The Niger Delta is known for its structural-stratigraphic plays and traps (Short and Stauble, 1967; Weber and Daukoru, 1975; Avbovbo, 1978; Doust and Omatsola, 1990; Tuttle *et al*., 1999; Haack *et al*., 2000; Mackenzie, 2005). The area of study is approximately 124.24 km^2 in size and has producing reservoir series tested by nine (9) wells.

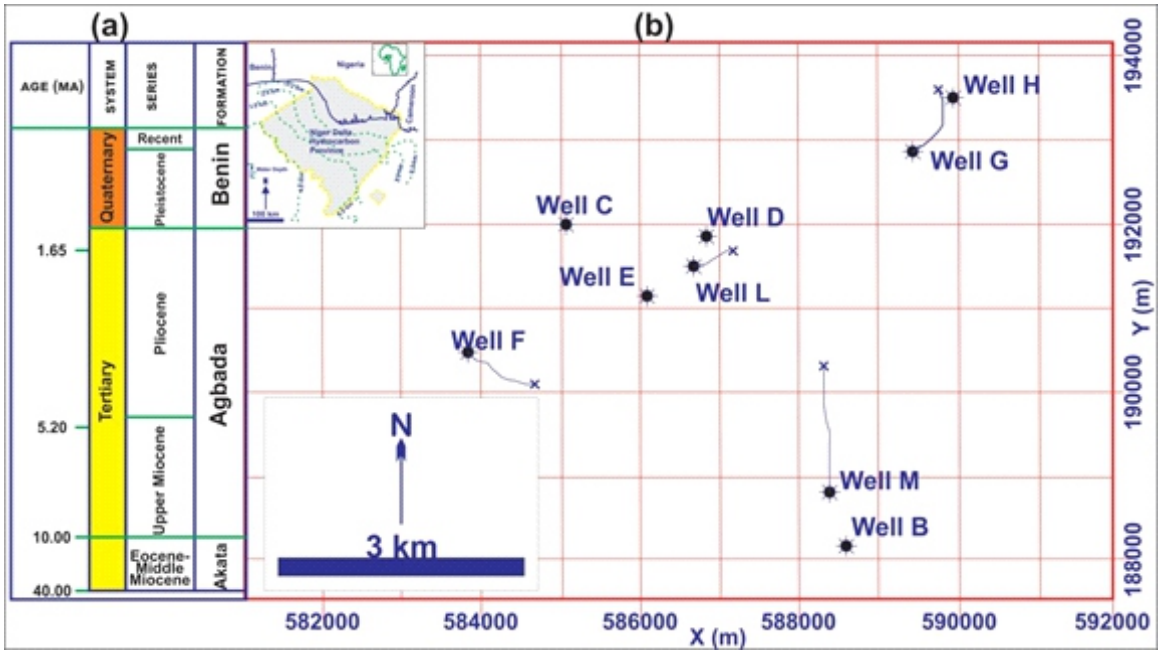

Figure 1: The study area showing (a) the stratigraphic column of Niger Delta (after Tuttle *et al*., 1999) (b) the base map of the study area with inset of the outline of the Niger delta petroleum province (after Petroconsultants, 1996).

DATABASE AND WORKFLOW

The database consists of (1) checkshot and deviation survey data from 9 wells; (2) 3D PreStack Time Migrated (PSTM) SEG-Y AVO substacks of near-angle (0-20), far-angle (20-35) structural partial stacks (Inline 156-500 Vs Crossline 1-401) with a bin spacing of 36.2645 x 25 m producing 138345 seismic traces and record length of 5.8 seconds; and (3) suite of logs - gamma ray, photoelectric factor, self potential, resistivity, sonic, density, neutron porosity, and ccalliper. The workflow is as shown in Figure 2. It follows a sequential, iterative and integrated procedure using a combination of Petrel™, Kingdom Suite (now IHS Kingdom Advanced™) and Hampson-Russell (STRATA module) software™ in order to achieve the objectives of the study. The Petrel and IHS Kingdom Advanced are suited for the general seismic and well log interpretation while the Hampson-Russell is essentially suitable for the AVO analysis. The logs were interpreted for lithostratigraphic correlation and petrophysics to establish petrophysical-to-seismic relationships and select reservoir of interest. The quantified petrophysical parameters include thickness (Net, Gross, NGR), porosity, and water saturation. Cut-offs were determined and applied to characterize and isolate net-pay zones that are of significance. 3D seismic-geologic framework was built while depth conversion was achieved by using synthetics derived from convolution of extracted wavelets (zero-phased) and reflectivity. The analysis of the AVO attributes and inversion sensitivity tests allowed for the generation of elastic and acoustic inversion attributes of the substacks. The resulting attributes and parameters were calibrated to known reservoir properties at well controls and validated for consistency. The integration of the attributes and parameters with 3D visualization was used to predict the distribution of reservoir property/heterogeneity, map new plays, generate prospects and appraise the hydrocarbon potential of the field.

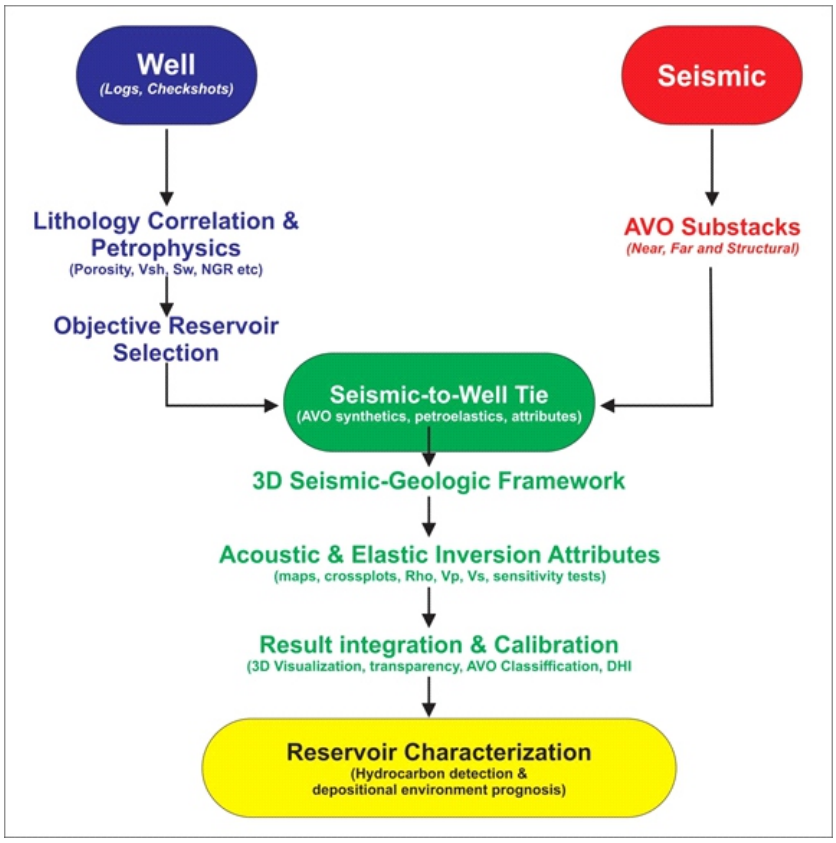

Figure 2: Study workflow.

THEORETICAL PRINCIPLES

Velocities

The exploration seismic method is based on the propagation of seismic waves across complex heterogeneous underground media. The propagation is basically dependent on the elastic deformation in shape and size caused when rocks are subjected to external forces. The wave energy at a planar surface partitions in the form of longitudinal p- and transverse s- waves. The particle motion associated with longitudinal (compressional) wave is known as p-wave and consists of alternating compression and rarefaction following wave propagation. It can travel through solids, liquid and gases all of which are compressible (k = 0) and has a velocity given by

$$\alpha = \left[\frac{\kappa + \frac{4}{3}\mu}{\rho}\right] \quad (1)$$

Where bulk modulus (k), shear modulus (μ) and density (ρ) are elastic parameters. The other wave is known as shear wave (s-wave) which has a frequency and velocity approximately half of p-wave's in the same medium and travels perpendicularly to the direction of propagation. It is usually the second event observed on seismic record. Liquids and gases do not allow shear wave propagation (μ = 0) and its velocity is given by:

$$\beta = \left[\frac{\kappa}{\rho}\right]^{\frac{1}{2}} \quad (2)$$

AVO approximations and inversion

The theory behind AVO (Zoeppritz, 1919; Knott 2007; Chopra and Castagna, 2014) is based on the assumption that between the planar interface of two homogeneous media (Figure 3a), angle of incidence, density, Poisson's ratio, p- and s- wave velocities have a significant effect on reflectivity (Equations 3-6).

$$A_1 cos\theta_1 - B_1 sin\phi_1 + A_2 sin\theta_2 - B_2 sin\phi_2 = A_0 cos\theta_1 \quad (3)$$

$$A_1 sin\theta_1 - B_1 cos\phi_1 - A_2 sin\theta_2 - B_2 cos\phi_2 = -A_0 sin\theta_1 \quad (4)$$

$$A_1 Z_1 cos2\phi_1 - B_1 W_1 sin2\phi_1 - A_2 Z_2 cos2\phi_2 - B_2 W_2 sin2\phi_2 = -A_0 Z_1 cos\phi_1 \quad (5)$$

$$A_1 \gamma_1 W_1 sin2\theta_1 - B_1 W_1 cos2\phi_1 + A_2 \gamma_2 W_2 sin2\theta_2 - B_2 W_2 cos2\phi_2 = -A_1 \gamma_1 W_1 sin2\theta_1 \quad (6)$$

Where $\gamma_i = \beta_i / \alpha_i$; $Z_i = \rho_i * \alpha_i$; $W_i = \rho_i * \beta_i$; $i = 1$ *or* 2; α= p-wave velocity; β= s-wave velocity; Z = acoustic impedance contrast for p-wave; W =

acoustic impedance for s-wave; θ_1 = p-wave incident angle; θ_2 = p-wave transmission angle; ϕ_1 = s-wave reflection angle; ϕ_2 = s-wave transmission angle.

However, in order to completely describe the partition of seismic energy at a reflecting horizon, the Equations (3-6) above are resolved for the following coefficients,

$$\frac{A_1}{A_0} = reflection\ coefficient\ for\ P-wave \quad (7)$$

$$\frac{A_2}{A_0} = transmission\ coefficient\ for\ P-wave \quad (8)$$

$$\frac{B_1}{A_0} = reflection\ coefficient\ for\ S-wave \quad (9)$$

$$\frac{B_2}{A_0} = transmission\ coefficient\ for\ S-wave \quad (10)$$

For a small amplitude contrast in elastic properties, Aki and Richards (2002) approximates the Zoeppritz as:

$$R(p) \cong \frac{1}{2}(1-4p^2\beta^2)\frac{\Delta\rho}{\rho} + \frac{1}{2cos^2\theta}\frac{\Delta\alpha}{\alpha} - 4p^2\beta^2\frac{\Delta\beta}{\beta} \quad (11)$$

Where R(p) is amplitude of p-wave reflection and $p = \sin\theta/\alpha_1$ = ray parameter. All other parameters retain their meanings as indicated in Equations (3-6). Equation 12 is a Shuey (1985) derivation of the linearized reflection coefficient for incident angle $\leq 30^{\circ}$.

$$R(\theta) = \boldsymbol{R_0} + \boldsymbol{G}\sin^2\theta + \boldsymbol{C}(\tan^2\theta - \sin^2\theta) \quad (12)$$

$$\boldsymbol{R_0} = \frac{1}{2}\left[\frac{\Delta\alpha}{\alpha} + \frac{\Delta\rho}{\rho}\right];$$

$$\boldsymbol{G} = \left[\frac{\frac{\Delta\alpha}{\alpha}}{\left[\frac{\Delta\alpha}{\alpha} + \frac{\Delta\rho}{\rho}\right]} - 2[1+B_0]\left[\frac{1-2\sigma}{1-\sigma}\right]\right]R_0 + \left[\frac{\Delta\sigma}{[1-\sigma]^2}\right]$$

and $\boldsymbol{C} = \frac{1}{2}\frac{\Delta\alpha}{\alpha}$

R(θ) is the reflectivity (or reflection coefficient) that varies with angle. $\mathbf{R_0}$ is the intercept (reflectivity at origin or at normal incidence); **G** is the AVO slope or gradient; **C** is the curvature that dominates at far offset, near the critical angle and is σ the Poisson's ratio (Sen, 2006). Acoustic impedance contrast at the interface influences the intercept (R_0), while the gradient G varies with changes in α, β, ρ and β/α. C only varies with α and contributes a very small proportion to the effects of amplitudes below angles ≈30°. Shear wave effect on reflection coefficients is large and noticeable at large incidence angles (Sen, 2006). In other words, the reflectivity series (Equation 12) has only the acoustic impedance contrast at near angle and a combination of acoustic and elastic impedance at farther angles.

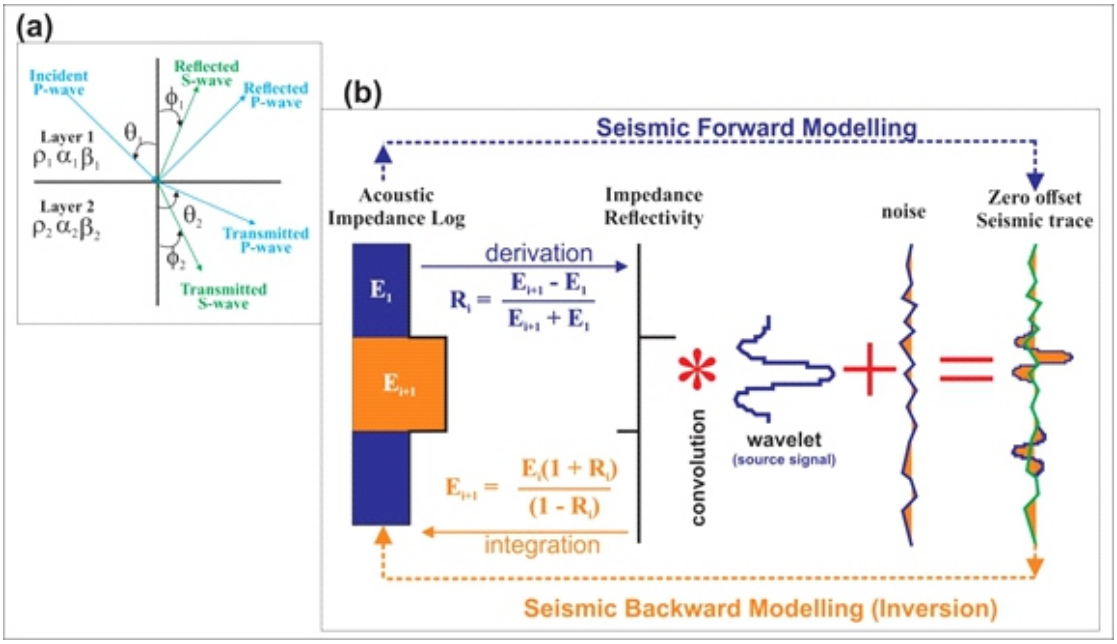

Figure 3: (a) Mode conversion from an incident P-wave arrival at the interface between two elastic media (After Sen, 2006) (b) Generalized inversion basic principle.

Generalized inversion principle

Inversion transforms 3D seismic data into its equivalent rock characteristics which can be, not limited to thickness, fluid and saturation. It resolves the individual impedance layers with the ultimate aim of improving reservoir characteristics prediction (Figure 3b). The acoustic impedance requires stacked p-wave and solves for density and velocity to predict lithology, thickness and porosity. The elastic impedance requires s-wave and solves for compressibility, shear strength and rigidity to predict litholog, thickness, porosity and saturation. Attribute requires any form of seismic data, acoustic and elastic impedance to glean seismic characters relevant to predicting lithology, thickness, porosity and saturation (Berge *et al.*, 2002).

The commonly adopted inversion algorithm and which is expected to be more accurate is that by wave-form fitting (Sen, 2006). The modelling involves the computation of synthetic traces at varying offsets and angles by the use of the convolutional model and iterative fitting of the synthetic traces with the real traces within acceptable intervals by minimizing equation 13. It usually starts by the pertubation of a low-frequency P-impedance model generated from seismic horizons and well log data (Ahhinav and Kharagpur, 2012; Sen, 2006).

$$T = \varphi_1 [S - W * R] + \varphi_2 [M - H * R] \quad (13)$$

where φ_1 and φ_2 are weights/coefficients, R is the reflection coefficient; W is the wavelet; S is the seismic trace; and M is the a priori impedance model. The final impedance is produced from the convolution of H and R, and * is the convolution operator. As [S - W * R] approaches the minimum, it approximates the seismic trace while as [M - H * R] approaches the minimum, it approximates the a priori impedance model (Hampson and Russell, 1999). This allows the log data to be honoured for low frequency and layered geology for high frequency leading to selection of an appropriate model with the least number of layers (Falebita *et al.*, 2019).

RESULTS AND DISCUSSION

Lithology correlation and petrophysics

The correlation of the hydrocarbon reservoirs encountered across eight (8) of the nine (9) available wells using gamma ray (GR) and resistivity logs are displayed in Figure 4. Table 1 indicates the characteristics of the reservoirs that contain hydrocarbon from the nine (9) wells available for the study area.

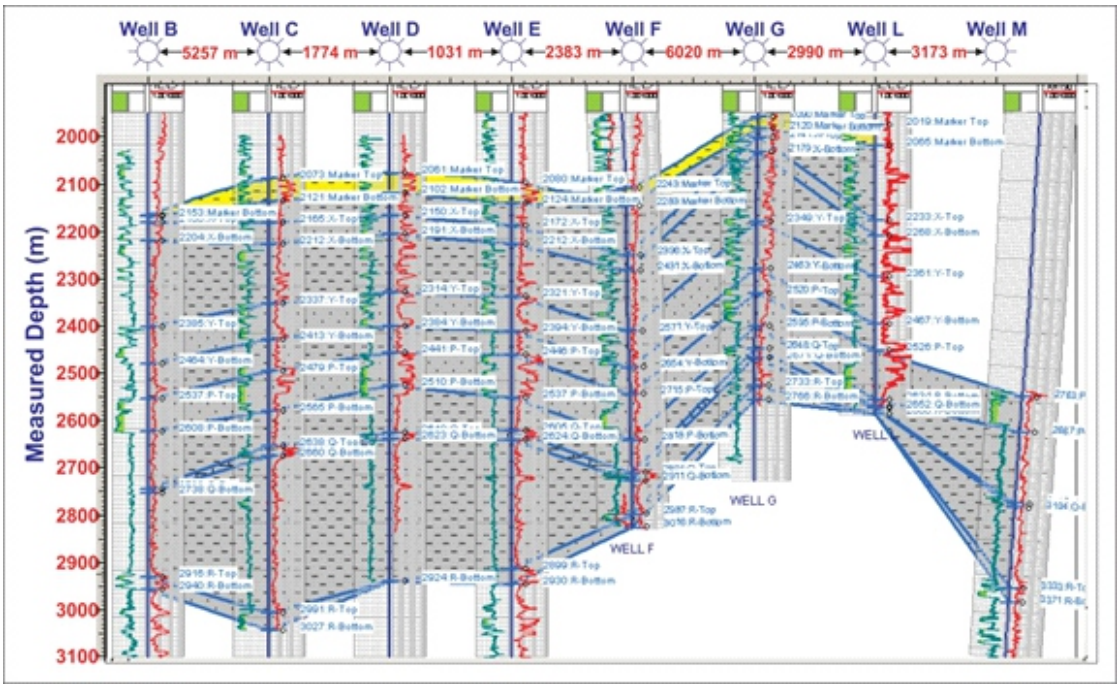

Figure 4: Lithostratigraphic correlation across wells.

The wells are labelled Well B, Well C, Well D, Well E, Well F, Well G, Well H, Well I, Well L and Well M while the reservoirs are labelled X, Y, P, Q, R, S, T and U. Reservoir X is the shallowest while Reservoir U is the deepest. Reservoirs X, Y, P and Q are found within upper channel and lobe complexes A while reservoirs R, S, T and U are found in lower channel and lobe complexes B (Figure 5). The subsea depths to the tops and bases of the reservoirs are indicated as Top TVDSS and Base TVDSS respectively. Table 2 summarizes the average petrophysical parameters of the reservoirs from all the wells. The average depth-to-the-top of the shallowest Reservoir X is about 2436 m, while that of the deepest reservoir U is about 2549 m. The gross thickness of the reservoirs varies from about 62 m in reservoir Q to about 89 m in reservoir T. However, the net-to-gross only varies between 88% and 91% of the gross thickness. This means the reservoirs are relatively clear of free of shale presence. Their porosity values only vary by 3% with reservoir U having the minimum of 23%, while 6 reservoirs (X, Y, P, Q, R and S) have the maximum of 26%. This means that most of the reservoirs have good porosity except for the few that have porosity less than 10%. The water saturation varies from 48% in reservoir S to about 85% in reservoir U. This clearly indicates that the hydrocarbon content in the reservoirs varies from 15% to 52%. For all the reservoirs, the NGR and PHIE do not vary widely but the SW does. In this study, however, Reservoir P is selected for further seismic-structural and AVO analyses. This is because it is encountered in more wells than other reservoirs and has a gas cap in addition to oil and water encountered in Well E (Figure 5a). Moreover, the AVO feasibility test (Figure 5b) confirms it as potential AVO objective target.

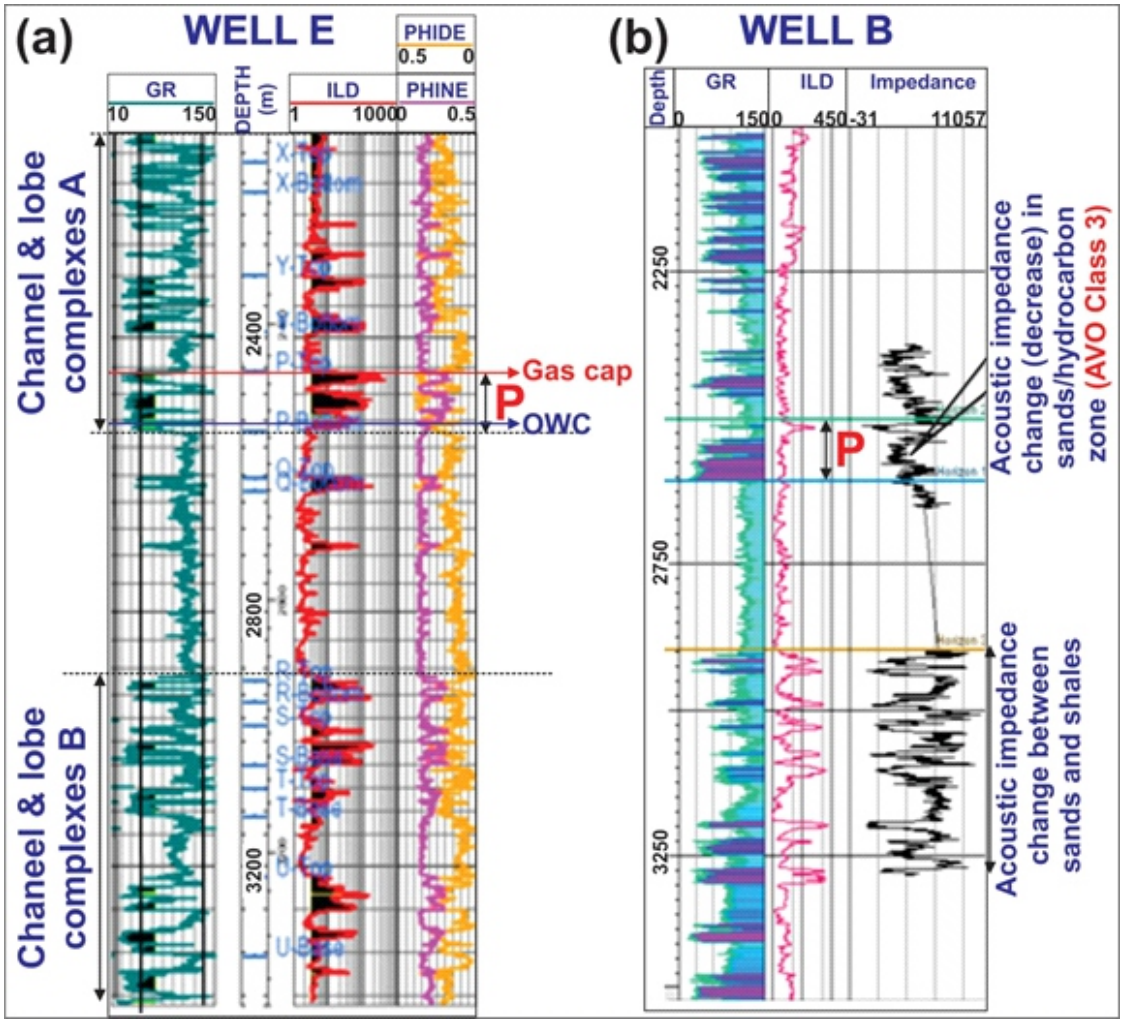

Figure 5: Delineated stratigraphic features and AVO characteristics from Wells E and B.

Table 1: Summary of evaluated petrophysical parameters by wells.

Well	Reservoir Sand	Top TVDSS (m)	Base TVDSS (m)	NGR	PHIE	SW
B	S	2997.00	3148.00	0.80	0.27	0.21
	T	3209.00	3320.00	0.84	0.28	0.60
C	Y	2352.70	2428.77	0.90	0.22	0.76
	P	2494.60	2580.28	0.91	0.24	0.55
	Q	2653.82	2675.66	0.88	0.26	0.31
D	X	2165.80	2206.00	0.83	0.21	0.54
	Y	2329.40	2399.60	0.85	0.22	0.55
	P	2456.84	2525.22	0.90	0.26	0.36
	Q	2625.62	2638.07	0.85	0.29	0.28
E	X	2188.07	2227.18	0.82	0.20	0.65
	Y	2336.16	2410.06	0.87	0.22	0.55
	P	2461.65	2552.33	0.88	0.26	0.26
	Q	2621.01	2639.81	0.83	0.26	0.29
	R	2914.76	2946.00	0.81	0.21	0.46
	S	2988.00	3055.00	0.81	0.21	0.40
	T	3097.00	3144.00	0.87	0.20	0.61
	U	3227.00	3299.00	0.84	0.19	0.54
F	X	2250.59	2283.00	0.75	0.26	0.87
	Y	2411.63	2488.08	0.88	0.26	0.88
	P	2544.47	2641.27	0.84	0.26	0.83
	Q	2711.60	2727.22	0.60	0.23	0.28
	R	2798.20	2825.65	0.78	0.22	0.87
G	X	1999.70	2031.50	0.83	0.26	0.53
	Y	2179.30	2279.00	0.83	0.26	0.56
	P	2330.70	2399.60	0.87	0.25	0.67
	Q	2447.50	2468.40	0.85	0.27	0.95
	R	2526.30	2556.90	0.74	0.25	0.93
H	X	2067.00	2130.00	0.88	0.27	0.52
	Y	2158.00	2265.00	0.87	0.26	0.50
	P	2327.60	2383.99	0.89	0.28	0.67
	Q	2437.00	2457.30	0.80	0.25	0.93
L	X	2176.15	2209.26	1.00	0.23	0.31
	Y	2296.32	2396.70	1.00	0.22	0.32
	P	2452.98	2555.80	0.92	0.25	0.30
M	P	2548.98	2623.98	0.87	0.23	0.85
	Q	2774.88	2783.28	0.61	0.21	0.87

Table 2: Average values of petrophysical parameters by reservoirs.

Reservoir	Top Depth (m)	Base Depth (m)	Gross Thickness (m)	NGR	Porosity	SW
X	2435.98	2513.78	77.81	0.88	0.26	0.56
Y	2446.17	2526.03	79.85	0.88	0.26	0.56
P	2493.23	2558.84	65.61	0.87	0.26	0.52
Q	2497.74	2559.77	62.03	0.87	0.26	0.56
R	2370.43	2446.46	76.04	0.89	0.26	0.55
S	2390.29	2469.90	79.61	0.91	0.26	0.48
T	2500.98	2589.89	88.91	0.89	0.24	0.58
U	2548.98	2623.98	75.00	0.87	0.23	0.85

Seismic-structural framework

Figure 6 is a far-stack seismic section indicating some structural features and seismic-to-well tie at Well B. The structural interpretation of the top of reservoir P (Figure 7) delineates a NW-SE major listric fault. The fault separates the field into two fault blocks named BA and BB leading to two main structural closures named A and B. Closure A is at the downthrown side while closure B is at the upthrown side of the fault. It appears that closure A was tested by wells C, E, and F and appraised by wells B and M, while closure B was tested by wells G and H and appraised by well D and L. These structural characteristics are common in the Niger delta petroleum province (Doust and Omatsola, 1989; Tuttle *et al*., 1999).

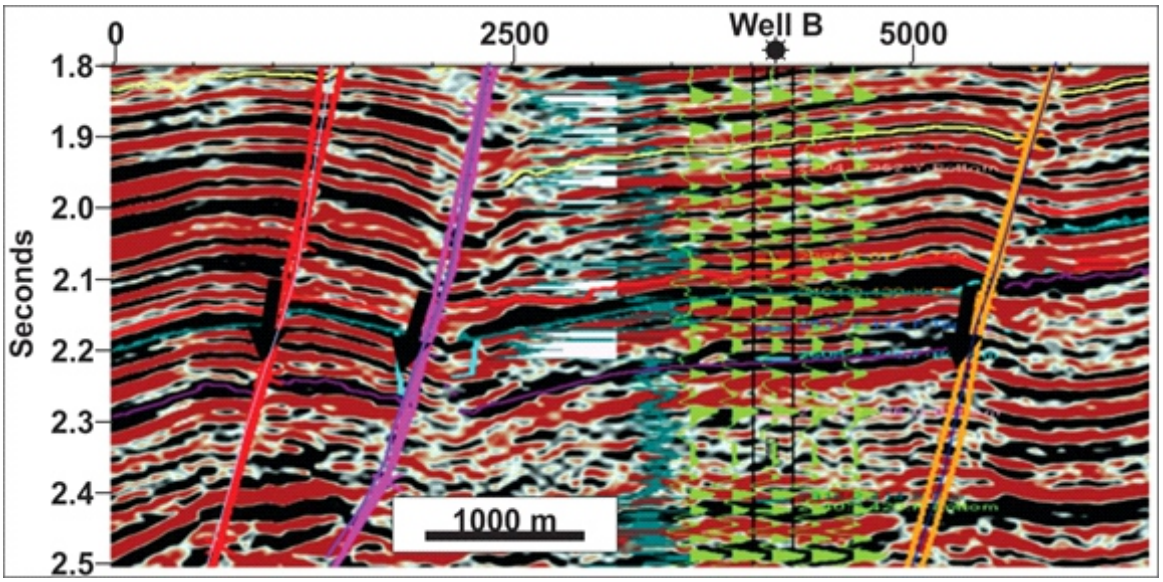

Figure 6: Far stack section indicating synthetic seismogram at Well B for seismic-to-well tie.

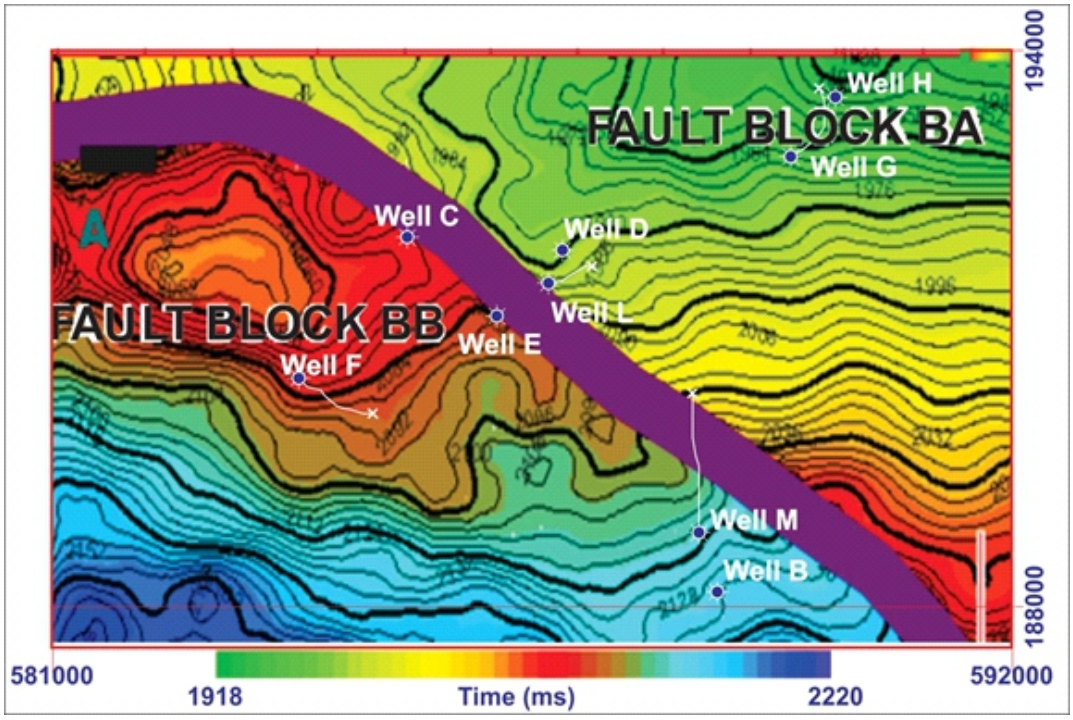

Figure 7: Time structural map of target reservoir P showing the two main fault blocks (BA and BB) in the study area.

Amplitude spectra and a priori impedance model

Figure 8a is a display of the amplitude spectra of the near and far angle stacks as well as their crossplots which highlight the spectral consistency of the angle stacks for AVO analysis.

Figure 8b is an a priori low frequency (~ 7Hz) pseudologs of absolute acoustic/elastic impedance values at each seismic trace. This reduces the non-uniqueness of the seismic solution (Russel and Hampson, 1991; Karim *et al*., 2016).

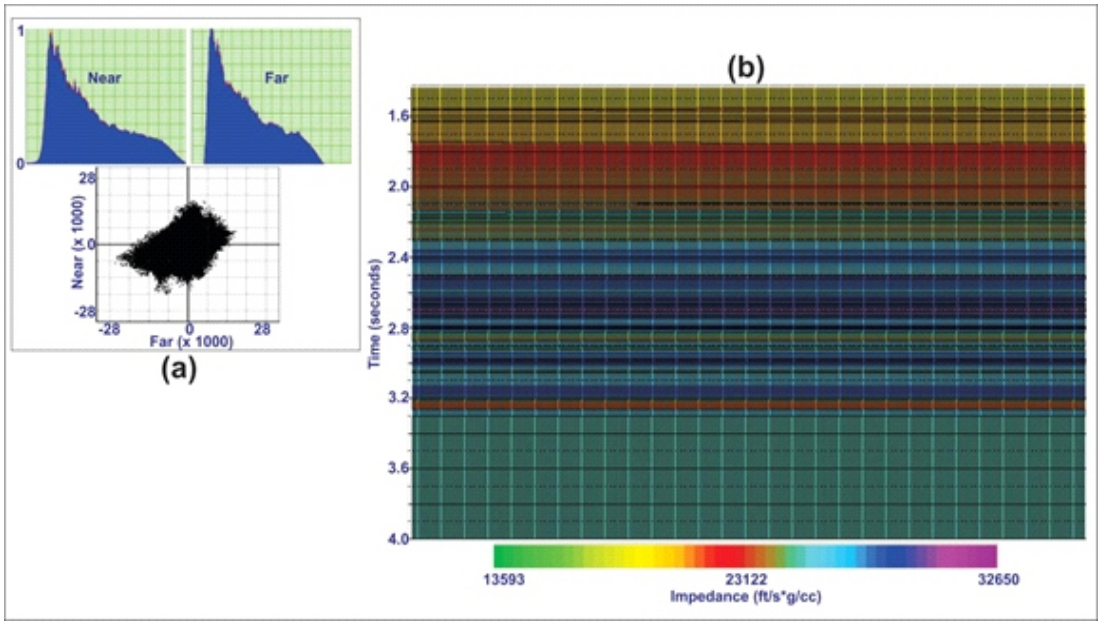

Figure 8: (a) The amplitude spectra of the near vs far angle stacks and (b) a priori P-impedance model generated for elastic inversion.

Acoustic and elastic inversion attributes

The direct inversion of the seismic traces (Figure 9a) is the recursive high frequency acoustic inversion (Figure 9b) obtained in the frequency domain. The inverted section highlights the gross thicknesses of the individual sand packages better than the original seismic section. However, it could not resolve the detailed reservoir heterogeneities (architecture) and the variation in the impedance with depth. This led to the application of the elastic inversion. Figure 9c is the result of the far stack elastic inversion. The fine layering associated with the seismofacies heterogeneities and shale breaks are clearly delineated. The low impedance (green-yellow-red) indicates sand (channelized lobe complexes and fans) while the high impedance (blue-to-purple) is diagnostic of shale. Figure 10 is the far-stack elastic inversion cube.

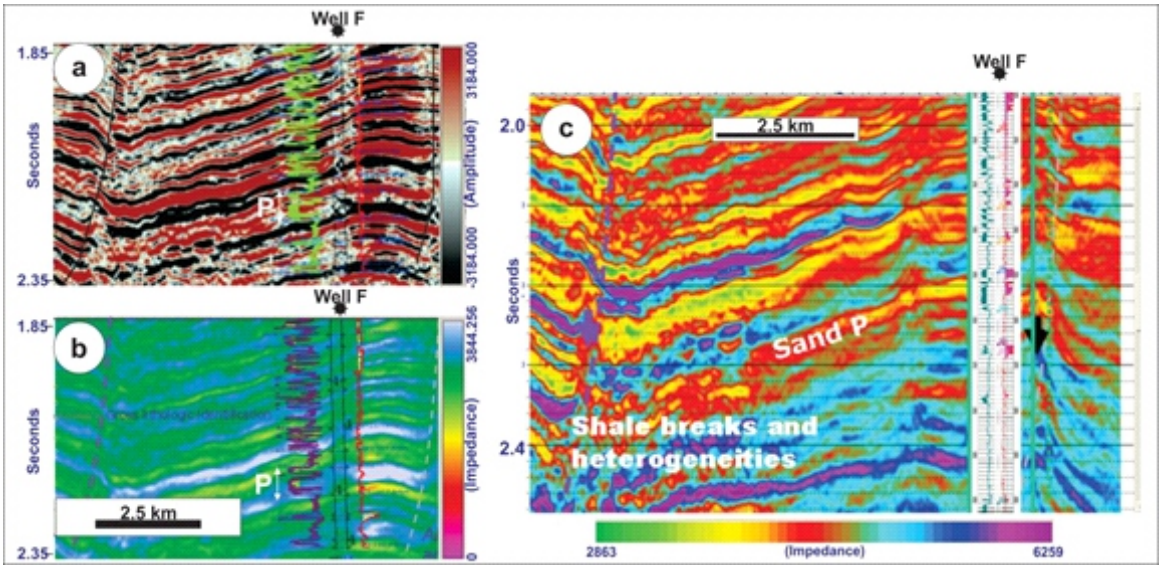

Figure 9: Far stack (a) uninverted seismic trace, (b) recursive high frequency acoustic inversion, and (c) elastic inversion section showing the seismofacies heterogeneities /shale breaks. The low impedance (green -yellow-red) indicates sand while the (blue to purple) high impedance is diagnostic of shale.

Depositional environment prognosis

Elastic inversion seismic attributes and the resultant geological models are driven by the environment of deposition. Figure 11 is an integrated deterministic elastic inversion model comprising the attributes, well logs and the interpretation based on sequence stratigraphic model (Catuneanu *et al*., 2011). It highlights the degree of fine lithologic layering and facies heterogeneities resulting from the sand architecture and shale breaks that create compartmentalization between the fans and multiple stacks of channel sand packages across the intervals of interest. The presence of the thick shale 360 m between 2552-2915 m TVD at Well E shows a marine environment with the maximum flooding surface (MFS) corresponding to the base of the P-Sand lobe complexes. The MFS is a product of sea level change and tectonics. The lobe complex was mapped as vertically stacked multiple channel deposits. The results showed the possibility of bypassed reservoirs due to the structural and stratigraphic complexity created by the growth fault and complex internal facie architecture and heterogeneities. The calibrated anomalously low elastic impedances are the hydrocarbon charged reservoirs.They have very good lateral and vertical seals and as such recommended for drilling. A well is proposed as indicated in Figure 11 to tap into the proximal fans beneath the maximum flooding surface. The deep plays continuity can be exploited in drilling wells away from the existing control wells to capture the lateral extent of the producing zones.

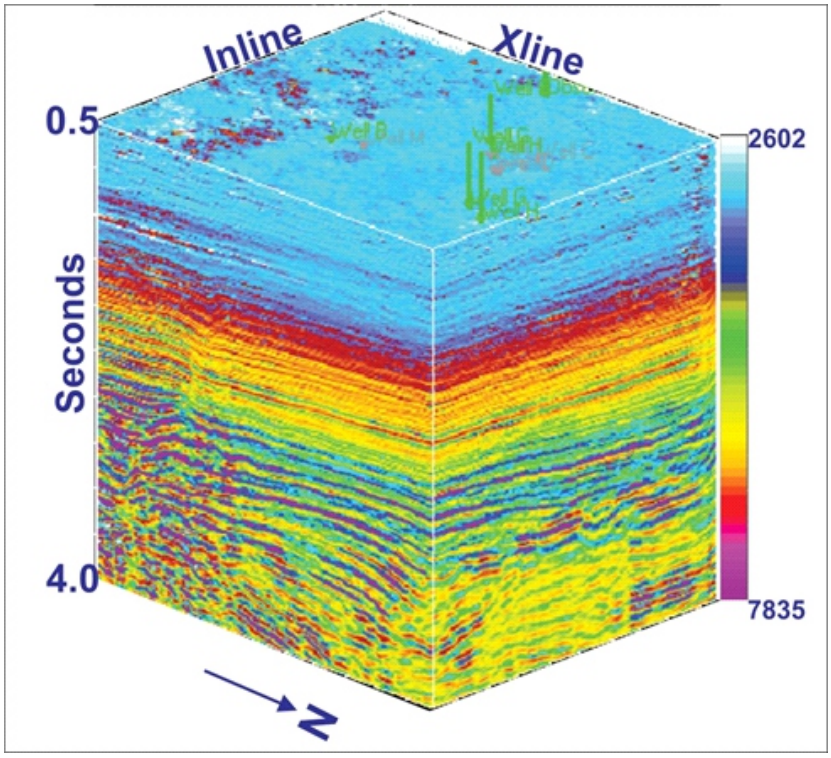

Figure 10: Generated Far stack elastic inversion cube.

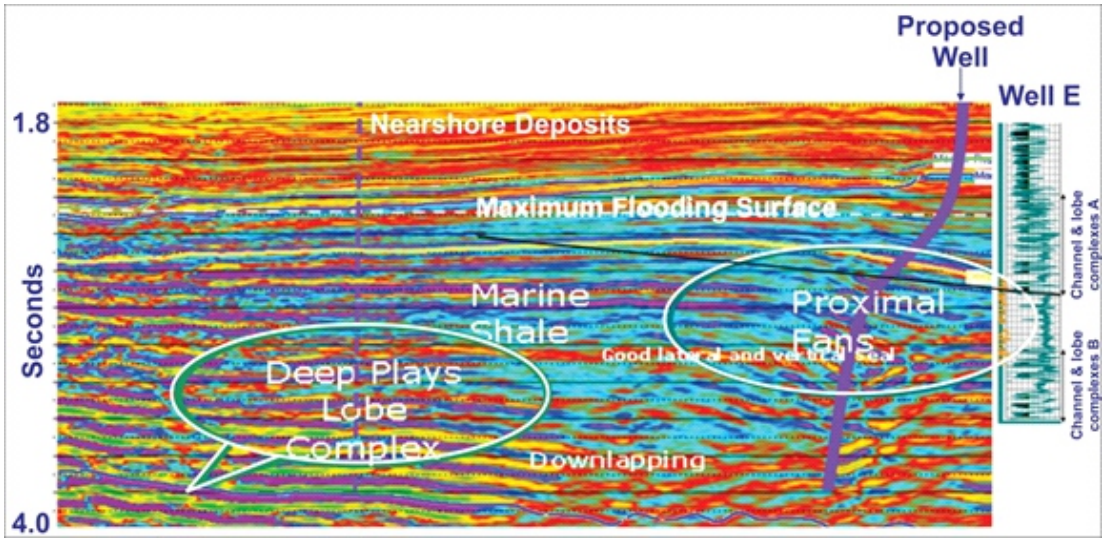

Figure 11: Far stack elastic inversion section showing the major sequence stratigraphic units and surfaces as well as proposed well.

CONCLUSION

The results obtained demonstrate the effectiveness of integrated multi-attribute seismic analysis and petrophysically constrained AVO-inversion for reservoir evaluation and assessment of the hydrocarbon prognosis within the area. Furthermore, the predictive capabilities of the attributes, particularly the AVO inversion (elastic parameter) volumes enhance the identification of the 3D outlines of the mapped hydrocarbon bearing channels and subtle stratigraphic bodies (channel, fans and lobes complexes). This improves the characterization of the reservoir sands and, consequently reduces the uncertainties associated with the prospects for economic decision making.

REFERENCES

Ahhinav, K.D. and Kharagpur, I.I.T. 2012. Reservoir Characterization using AVO and Seismic Inversion Techniques. 9th Biennial International Conference and Exposition on Petroleum Geophysics, Hyderabad, P205.

Aikulola U.O. and Olorunniwo, M.A. 2004. Seismic Attributes in subsurface Hydrocarbon Reservoir Mapping: A case history of 3D seismic interpretation over Timbe Field, Niger Delta. Nigerian Association of Petroleum Explorationists. Book of Abstracts, pA4.

Aki, K., and Richards, P.G. 2002: Quantitative Seismology, 2nd Edition, Sausalito, California. University Science Books.

Avbovbo, A.A. 1978. Tertiary Lithostratigraphy of the Niger Delta. *American Association of Petroleum Geologists*, 62: 295-306.

Bahorich, M. and Farmer, S. 1995. The Coherence cube. *The Leading Edge*, 14: 1053-1058. doi: 10.1190/1.1437077

Berge, T.B., Aminzadeh, F., De Groot, P. and Oldenziel, T. 2002. Seismic inversion successfully predicts reservoir, porosity, and gas content in Ibhubesi Field, Orange Basin, South Africa. *The Leading Edge*, 21: 338-348. doi: 10.1190/1.1471595

Bose, A., Singh, V., Josyulu, B.S. and Mahesh, C. 2004. A case study of stratigraphic and lithologic interpretation of thin reservoirs through as integrated approach. *The Leading Edge*, 23: 966-972. doi:10.1190/1.1813354

Brown, P., Odufisan, W., Eze, M., Fashbaugh, E., Foreman, L., Kenney, P., Saltzer, R. and Sokn, A. 2004. Integrated approaches expedites Geologic models and Well planning in the Bose Deepwater Development OPL 209, Nigeria. Nigerian Association of Petroleum Explorationists Book of Abstracts. pA10.

Catuneanu, O., Galloway, W.E., Kendall, C.G., Miall, A.D., Posamentier, H.W., Strasser, A, and Tucker, M.E. 2011. Newsletters on Stratigraphy, 44(3): 173-245. doi: 10.1127/0078-0421/2011/0011

Chopra S, and Castagna, J. P 2014. Zoeppritz Equations and their Approximations. AVO. Society of Exploration Geophysicists, 16. doi: 10.1190/1.9781560803201

Chopra S, and Marfurt KJ 2005. Seismic attributes - a historical perspective. *Geophysics*, 70(5), p1SO-Z82. doi: 10.1190/1.2098670

Chopra, S. and Pruden, D. 2003. Multiattribute seismic analysis on AVO-derived parameters—A case study. *The Leading Edge*, 22: 998-1002. doi: 10.1190/1.1623640

Connolly, P. 1999. Elastic Impedance. *The Leading Edge*, 18(4): 438-452. doi: 10.1190/1.1438307

Doust, H., and Omatsola, E. 1989. Niger Delta In: Edwards, J.O. and Sandtogrossi, P.A. eds. Divergent/Passive Margin Basins, Book Chapter, AAPG Memoir 48: Tulsa. *American Association of Petroleum Geologists Bulletin Memoir*, 62: 234-248. doi: 10.1306/M48508C4

Eissa, M.A. and Castagna, J.P. 2003. Case Study: AVO analysis in a high-impedance Akota sandstone (Pennsylvanian), North Arkoma Basin, Mclntosh County, Oklahoma. *The Leading Edge*, 22(10): 988-997. doi: 10.1190/1.1623639

El-Mowafy, H and Marfurt, K.J. 2008. Structural interpretation of the middle Frio Formation using 3D seismic and well logs. An example from the Texas Gulf Coast of the United States. *The Leading Edge*, 27(7): 840-854. doi: 10.1190/1.2954023

Falebita, D.E., Saviour, M.K., Jaiyeola, O.A., Ojo, A.A. Adepelumi 2019. Discrimination of post-stack bright spots using AVO and model-based inversion technique, Coastal Swamp Niger Delta, Nigeria - A case study. International M. K. *Journal for Petroleum Processing, Petrochemistry and Coal Processing*, 61(6): 1468-1478.

Haack, R.C., Sundaraman, P., Diedjomahor, J.O., Xiao, H., Gant, N.J., May, E.D. and Kelsch, K. 2000. Niger Delta Petroleum Systems, Nigeria, Book Chapter, AAPG Memoir 73: Tulsa. *American Association of Petroleum Geologists Bulletin*, 62: 234-248.
doi: 10.1306/M73705C16

Hampson, D. and Russell, B., (1999). Hampson Russell, STRATA Theory. Hampson-Russell Software Services Limited, 44-60.

Hilterman, F. 1990. Is AVO the seismic signature of lithology? A case of ship Shoal south addition. *The Leading Edge*, 9(6): 15-22.
doi: 10.1190/1.1439744

Huang, X. 2001. Integrating time-lapse seismic with production data: A tool for reservoir engineering. *The Leading Edge*, 20(10): 1148-1153.
doi: 10.1190/1.1487247

Karim S.U., Islam M.S., Hossain, M.M. and Islam, M.A. 2016. Seismic reservoir characterization using model-based post-stack seismic inversion: In case of Fenchugani gas field, Bangladesh. *Journal of the Japan Petroleum Institute,* 59(6): 283-292.
doi: 10.1627/jpi.59.283

Knott, C.G. 2007. Reflexion and Refraction of Elastic Waves, with Seismological Applications, Classics of Elastic Wave Theory, Michael A. Pelissier, Henning Hoeber, Norbert van de Coevering, Ian F. Jones.
doi: 10.1190/1.9781560801931.ch3k

Liephart, D.J., and Hart, B.S. 2001. Comparison of linear regression and a probabilistic neural network to predict porosity from 3D seismic attributes in Lower Brushy Canyon channelled sandstones, southeast New Mexico. *Geophysics*, 66(5): 1349-1358.
doi: 10.1190/1.1487080

Michael, D.B. and Castagna, J.P. 2003. Application of Special decomposition to gas basin and Mexico. *The Leading Edge*, 22(11): 1130-1134.
doi: 10.1190/1.1634918

Mukerji, T., Avseth, P., Mavko, G., Takahashi, I. and González E.F. 2001. Statistic rock physics: Combining rock physics, information theory, and geostatistics to reduce uncertainty in seismic reservoir characterization. *The Leading Edge*, 20(3): 313-319.
doi: 10.1190/1.1438938

Partyka, G., Gridley, J., and Lopez. 1999. Interpretational applications of spectral decomposition in reservoir characterization. *The Leading Edge*, 18(3): 353-361.
doi: 10.1190/1.1438295

Paulo, J., Gilberto, R. and Spínola, M. 2003. Spectral Decomposition Reveals Geological Hidden Features in the Amplitude Maps from a Deepwater Reservoir in the Campus Basin, SEG Technical Program Expanded Abstracts, 1740-1743.
doi: 10.1190/1.1817646

Petroconsultants, 1996: Petroleum exploration and production database: Houston, Texas, Petroconsultants, Inc., database available from Petroconsultants, Inc., P.O. Box740619, Houston, TX 77274-0619.

Rauch-Davies M., Efrain M. H. and Villasenor, R.V. 2003. A seismic attributes catalogue for detecting hydrocarbons in the Macuspana Basin, Mexico. SEG Technical Program Expanded Abstracts, 1748-1750.
doi: 10.1190/1.1817648

Russell, B., and Hampson, D. 1991. Comparison of post-stack seismic inversion. *EG Technical Program Expanded Abstracts*, 876-878.
doi: 10.1190/1.1888870

Russell, B., Hampson, D., Schuelke, J., and Quirern, J. 1997. Multiattribute Seismic Analysis. *The Leading Edge*, 16: 1439-1443.
doi: 10.1190/1.1437486

Schuelke, J.S., Quirein, J.A., and Pita, J.A. 1998. Prediction of Reservoir Architecture and Porosity Distribution Using Multiple Seismic Attributes and Neural Networks. Paper Presented at the Offshore Technology Conference, Houston.
doi: 10.4043/8600-MS

Sen, M.K. 2006. Seismic inversion. Society of Petroleum Engineers Primer Series, SPE, USA. 120 pp.

Short, K.C. and Stauble, A.J. 1967. Outline of Geology of Niger Delta. *AAPG Bulletin*, 51 (5): 761–779,
doi: 10.1306/5D25C0CF-16C1-11D7-8645000102C1865D

Shuey, R.T. 1985. A simplification of the Zoeppritz equations. *Geophysics*, 50: 609-614.
doi: 10.1190/1.1441936

Soldo, J., Lenge, D., Sigismondi, M., Telles, A. S., Sena, A. G., Smith, T. 2001. 3D AVO and seismic inversion in María Inés Oeste field, Santa Cruz, Argentina, a case study. SEG Technical Program Expanded Abstracts, 197-200.
doi: 10.1190/1.1816527

Tuttle, M.L.W., Carpentier, R.R. and Brownfield M.E. 1999. Tertiary Niger Delta (Akata-Agbada) Petroleum System, Niger Delta Province, Nigeria, Cameroon, and Equatorial Guinea, Africa. Open File Report 99-50-H, Chapter A, 1-44.

Weber, K.J. and Daukoru, E.M. 1975. Petroleum Geology of Niger Delta. 9th World Petroleum Congress Proceedings, 5(2): 209-221.

Zoeppritz, K. 1919. Erdbebenwellen VIII B, Uber Reflexion ad Durchgang seismischer Wellen durch Unstetigkeitsflachen. *Gottinger Nachr.,* 1: 66-84.